24p

Iron abundance and magnetic permeability of the moon

by

Curtis W. Parkin

Department of Physics, University of Santa Clara
Santa Clara, California 95053

William D. Daily

Department of Physics and Astronomy, Brigham Young University
Provo, Utah 84602

Palmer Dyal

NASA-Ames Research Center
Moffett Field, California 94035

Short title: Iron abundance in the moon

Abstract—A larger set of simultaneous data from the Apollo 12 lunar surface magnetometer and the Explorer 35 Ames magnetometer are used to construct a whole-moon hysteresis curve, from which a new value of global lunar permeability is determined to be $\mu = 1.012 \pm 0.006$. The corresponding global induced dipole moment is 2.1×10^{18} gauss-cm^3 for typical inducing fields of 10^{-4} gauss in the lunar environment. From the permeability measurement, lunar free iron abundance is determined to be 2.5 ± 2.0 wt. %. Total iron abundance (sum of iron in the ferromagnetic and paramagnetic states) is calculated for two assumed compositional models of the lunar interior: a free iron/orthopyroxene lunar composition and a free iron/olivine composition. The overall lunar total iron abundance is determined to be 9.0 ± 4.7 wt. %. Other lunar models with a small iron core and with a shallow iron-rich layer are discussed in light of the measured global permeability. Effects on permeability and iron content calculations due to a possible lunar ionosphere are also considered.

INTRODUCTION

Theoretical calculations of whole-moon iron abundance have been made by several investigators, often based on meteorite compositional models. Previous estimates for total iron abundance have generally been ~ 10% by weight (Urey, 1962; Reynolds and Summers, 1969; Urey and MacDonald, 1971; Wänke et al., 1973).

Emplacement of a network of magnetometer experiments on the lunar surface by Apollo astronauts in 1969-1972 has allowed investigation of lunar iron content and magnetic permeability, using in situ magnetic field measurements made simultaneously by instruments on the lunar surface and in orbit near the moon. From these simultaneous measurements whole-moon hysteresis curves can be constructed, from which global magnetic permeability can be calculated. (Behannon (1968) previously had calculated an upper limit of 1.8 for global permeability using measurements of a single lunar orbiting magnetometer.) The dual-magnetometer method was first employed by Dyal and Parkin (1971), who calculated whole-moon relative magnetic permeability to be $\mu = 1.03 \pm 0.13$. The uncertainty in this value was later reduced to $\mu = 1.029 \pm \begin{matrix} 0.024 \\ 0.019 \end{matrix}$ by Parkin et al. (1973). This measured permeability was used to calculate ferromagnetic free iron in the moon to be 5 ± 4 wt.%, and total iron in the moon to be 9 ± 4 wt.%.

In this paper the earlier work of Parkin et al. (1973) is extended. New values of global permeability, free iron, and total iron are determined using more data, improved statistical techniques, and better quantitative knowledge of the plasma-magnetic field environment of the moon. New hysteresis curves are plotted using a total of 2703 sets of magnetic field averages of data measured simultaneously by the Apollo 12 lunar surface magnetometer and the lunar orbiting Explorer 35 magnetometer. Slopes of

the hysteresis curves are used to calculate magnetic permeability of the moon, from which we calculate free iron abundance in the lunar interior. Then we calculate total iron abundance of the moon for assumed free iron/paramagnetic mineral compositions of the lunar interior. Also, we discuss other lunar models, one with an iron core and another with an iron-rich layer, in light of the measured global lunar permeability. Finally, Russell et al. (1974) have recently made permeability calculations using data from a single magnetometer, the Apollo 15 subsatellite magnetometer orbiting at an altitude about 100 km above the moon. The results to date indicate the possible existence of a lunar ionosphere between the lunar surface and the subsatellite orbit. We consider the effects of such an ionosphere, should its existence be proved, upon the lunar magnetic permeability and iron abundance results.

EXPERIMENTAL TECHNIQUE

During times when the moon is immersed in an external magnetic field which is spatially and temporally uniform, and plasma interaction effects are minimized, the total magnetic field $\underline{B}$ measured at the lunar surface by an Apollo magnetometer is expressible as

$$\underline{B} = \mu \underline{H} = \underline{H} + 4\pi\underline{M} \qquad (1)$$

where $\underline{H}$ is the external magnetizing field and $\underline{M}$ is the magnetization field induced in the permeable lunar material (see Fig. 1). The relative magnetic permeability is $\mu = 1 + 4\pi k$, where k is magnetic susceptibility in emu/cm^3. (In equation (1) the remanent field at the surface site is subtracted out for simplicity.) The total surface field $\underline{B}$ is measured by a lunar surface magnetometer (LSM) located at the Apollo 12 site on the moon (selenographic

coordinates 23.4° W. longitude, 3.0° S. latitude). LSM instrument properties are described in detail by Dyal et al. (1970) and summarized in a companion paper in this volume (Dyal et al., 1974). Simultaneous measurements of the geomagnetic tail field $\underline{H}$ are made by the lunar orbiting Explorer 35 Ames magnetometer, which orbits the moon with 0.5 R_m periselene and 5 R_m aposelene at a period of 11.5 hours. Characteristics of the Explorer 35 magnetometer are outlined by Sonett et al. (1967).

To determine iron content and magnetic permeability of the moon, we first construct a lunar B-H hysteresis curve using simultaneous measurements of the magnetizing field $\underline{H}$ external to the moon and the total magnetic induction $\underline{B}$ on the lunar surface. The slope of the hysteresis curve is then determined and the whole-moon initial permeability is calculated. This value is called the "initial" permeability because it is associated with the B-H hysteresis curve at very small magnetizing field $\underline{H}$ (order of 10^{-4} Oe). At these small field values, the characteristic "S" shape of the hysteresis curve degenerates to a straight line through the origin (Ellwood, 1934). Then from the global permeability, iron abundance in the lunar interior is determined as a function of thermal and compositional models of the lunar interior.

MAGNETIC ENVIRONMENT IN THE GEOMAGNETIC TAIL

In different regions of a lunar orbit (see Fig. 2), the magnetic environment of the moon can have distinctly different characteristics. Conditions desirable for analysis of lunar permeability and iron content exist in regions of the geomagnetic tail where the earth's magnetic field is spatially uniform and temporally constant, and effects of plasma currents are negligible.

Fig. 2

The geomagnetic tail is formed due to an interaction of the earth's permanent dipole field with the plasma flowing radially outward from the sun at an average velocity of $\sim$ 400 km/sec; in effect, the earth's field is swept back into a cylindrical region (the geomagnetic tail) on the earth's antisolar side. At the distance where the moon's orbit intersects the tail, the field magnitude is $\sim$ 10 gammas (10^{-4} Oe). Substructure of the tail consists of two "lobes": the upper or northward lobe has its magnetic field pointing roughly toward the earth, whereas the lower lobe field points away from the earth. The moon can pass through either or both lobes, depending upon the characteristics of the particular orbit, the geomagnetic dipole axis orientation, and perturbations of the geomagnetic field by solar wind pressures.

Data must be carefully chosen in the geotail so that interaction modes and induction modes other than global magnetization, are minimized. In general, it is possible that the total measured surface field $\underline{B}$ can include field contributions in addition to the geomagnetic field $\underline{H}$ and the magnetization field $\underline{M}$ induced in permeable lunar material. These other possible contributing field modes, some of which are very important in regions of the lunar orbit outside the geomagnetic tail, are the following: (1) the steady remanent field $\underline{B}_R$ due to permanently magnetized subsurface materials near the Apollo magnetometer site, (2) the toroidal field $\underline{B}_T$ resulting from transverse magnetic (TM) induction, (3) the poloidal field $\underline{B}_P$ resulting from transverse electric (TE) induction, (4) the field $\underline{B}_F$ associated with dynamic interaction between plasma flow and the above lunar fields, and (5) the field $\underline{B}_D$ associated with plasma diamagnetic currents. We examine here each of these possible fields to assess its impact on our study of the lunar magnetization field.

The remanent field $\underline{B}_R$ will not affect the hysteresis slope measurement. Since $\underline{B}_R$ is constant, its components added to equation (1) would, for hysteresis curves plotted for the separate field components of $\underline{B}$ and $\underline{H}$, simply result in a shift of the hysteresis curve away from the origin without altering the slope. Indeed, the radial component of $\underline{B}_R$ at the Apollo 12 site has been subtracted out of the lunar hysteresis curve presented in Fig. 3.

The toroidal mode $\underline{B}_T$ would result from currents driven in the lunar interior by a motional electric field $\underline{E}_m \propto \underline{V} \times \underline{H}$, where $\underline{V}$ is relative velocity of the moon with respect to the ambient bulk plasma flow. This type of field has not been detected within experimental error by lunar magnetometers (Dyal and Parkin, 1971) even in the solar wind, where $V \sim 400$ km/sec, much faster than the moon could move relative to the geomagnetic tail field during quiet times (lunar orbital velocity is 1 km/sec and geomagnetic tail motional velocity is generally $\sim$ 70 km/sec (Mihalov et al., 1970)). Furthermore, $\underline{B}_T$ is everywhere toroidal to $\underline{E}_m$ and tangential to the lunar surface (Schubert and Schwartz, 1969; Sill and Blank, 1970); therefore, contaminating effects of this induction mode can be neglected by use of only the radial components of $\underline{B}$ and $\underline{H}$ in our hysteresis curve analysis.

The induced poloidal field $\underline{B}_p$ results when time-dependent fluctuations of the field external to the moon ($\partial \underline{H}/\partial t$) drive eddy currents in the lunar interior. $\underline{B}_p$ is the dominant induction mode during times when the moon is immersed in the turbulent, rapidly changing solar wind field; however, in the limit of low-frequency or small-amplitude driving field fluctuations, as in the tail, $\partial \underline{H}/\partial t \rightarrow 0$ and poloidal induction vanishes. Therefore data-selection restrictions are placed on peak-to-peak variations of surface and external fields (to be discussed later) to eliminate data obviously

contaminated by eddy current fields. Furthermore, since global induced $\underline{B}_p$ fields have dipolar symmetry about the direction of $\partial\underline{H}/\partial t$, rather than $\underline{H}$, poloidal contamination would tend to scatter hysteresis curve data rather than change the hysteresis curve slope.

When the moon is in the free-streaming solar wind outside the geomagnetic tail, the dynamic interaction fields ($\underline{B}_F$) caused by the interaction between solar wind plasma and the lunar surface fields $\underline{B}_R$ have been found to be $\leq$ 16 gammas at the Apollo 12 site (Dyal et al., 1973). Plasma streaming pressure responsible for compression of surface fields is $(1/2)N_i m_p V^2$, where N_i is proton number density, m_p is the proton mass, and V is the plasma bulk speed. We assume that the typical plasma speed in the tail is characterized by the average magnetopause motions which are about 70 km/sec (Mihalov et al., 1970). Deep in the magnetotail lobes the plasma density is substantially below the density of $0.1/cm^3$ measured in the plasma sheet (Rich et al., 1973). Therefore the plasma-field interaction in the geotail should be at least 10^3 times weaker than in the free-streaming solar wind and can be neglected.

Another possible contaminating field is that due to plasma diamagnetism. As plasma particles spiral about the magnetic field lines $\underline{H}$, their motion induces a field ($\underline{B}_D$) which opposes $\underline{H}$. Plasma diamagnetism in the solar wind has been measured (Colburn et al., (1967); Ness et al., (1967)) as a field magnitude change of about 1.5 gammas by comparing Explorer 35 measurements in the solar wind with those in the plasma void on the antisolar side of the moon. Explorer 35 is unable to measure $\underline{B}_D$ directly in the plasma sheet of the geomagnetic tail, however, since there is no well defined plasma void created by the moon in the tail comparable to the antisolar cavity formed in the solar wind. An Apollo magnetometer on the lunar surface

should be shielded (at least partially) from extralunar diamagnetic effects; indeed, we have examined extensive data taken when the moon is near the neutral sheet, and we have seen differences as much as 2 gammas in fields measured by Apollo 12 LSM and Explorer 35. These field differences are directed such that they oppose the direction of the earth's field $\underline{H}$, characteristic of diamagnetic fields. We have found that we can minimize the inclusion of plasma diamagnetic fields in our hysteresis curve analysis by eliminating all data for which the measured Explorer 35 field magnitude $|\underline{H}| < 6 \times 10^{-5}$ Oe. This data selection criterion is applied so that only data from regions deep in the tail lobes are utilized.

Diamagnetism in the external environment produces the same effect in hysteresis-curve analysis as does paramagnetism in the lunar interior, i.e., paramagnetism determined for the moon is only relative to that of the lunar environment. Therefore if diamagnetic field data are included in the radial B-H hysteresis curve analysis, the measured global permeability will be higher than the true lunar permeability. In our earlier work (Parkin et al., 1973), the calculated permeability was higher than in this paper, due in part to inclusion of some plasma sheet data in the analysis.

MAGNETIC PERMEABILITY OF THE MOON

Magnetic permeability and iron abundance of the moon are calculated by analysis of magnetization fields induced in the permeable material of the moon. When the moon is immersed in an external field it is magnetized; the induced magnetization is a function of the distribution of permeable material in the interior. Under the assumption that the permeable material in the moon is predominately free iron and iron-bearing minerals, the lunar iron abundance can be calculated from the lunar permeability for assumed compositional models of the interior. Since the

amount of iron present in the lunar interior should be consistent with the measured global magnetic permeability, the permeability in effect places a constraint on the physical and chemical composition of the moon's interior. In this section we calculate global magnetic permeability of the moon. Lunar iron abundance will be determined from the permeability results in the following section.

Theory

For the lunar permeability and iron abundance analysis we use a two-layer lunar model (see Fig. 1). We assume that free iron and chemically combined iron in the Fe^{2+} (ferrous) state are responsible for the magnetic permeability of the lunar interior, and we model the moon with a homogeneous paramagnetic rock matrix (olivine and orthopyroxene models will be used), in which free metallic iron is uniformly distributed. Since the susceptibility of free iron changes several orders of magnitude at the iron Curie temperature (T_c), a two-layer model is used with the core-shell boundary R_c at the Curie isotherm. For $R > R_c$, $T < T_c$, and for $R \leq R_c$, $T > T_c$. Therefore, for $R > R_c$ any free iron will be ferromagnetic, while at greater depths where $T > T_c$, the free iron will be paramagnetic.

For the two-layer lunar permeability model illustrated in Fig. 1 the total field at the outer surface of the sphere is expressed (see Parkin et al., 1973):

$$\underline{B} = H_x(1 + 2G)\,\hat{x} + H_y(1-G)\,\hat{y} + H_z(1-G)\,\hat{z} \qquad (2)$$

where

$$G = \frac{(2\eta+1)(\mu_1-1) - \lambda^3(\eta-1)(2\mu_1+1)}{(2\eta+1)(\mu_1+2) \quad 2\lambda^3(\eta-1)(\mu_1-1)} \qquad (3)$$

Here $\eta = \mu_1/\mu_2$; μ_1 and μ_2 are relative permeability of the shell and core, respectively. Again, H_i are components of the geomagnetic tail field external to the moon, measured by the lunar orbiting Ames Explorer 35 magnetometer; $\underline{B}$ is measured by the Apollo 12 lunar surface magnetometer. The permeability exterior to the sphere is $\mu_o = 1$, that of free space; $\lambda = R_c/R_m$; R_c and R_m are radius of the core and the moon, respectively. Equation (2) expresses the total surface field in a coordinate system which has its origin on the lunar surface at an Apollo magnetometer site: $\hat{x}$ is directed radially outward from the lunar surface, and $\hat{y}$ and $\hat{z}$ are tangential to the surface, directed eastward and northward, respectively.

A plot of any component of equation (2) will result in a B - H hysteresis curve. Equation (3) relates the slope of the hysteresis curve to the lunar permeability. The average whole-moon permeability μ is calculated from the hysteresis-curve slope by setting $\mu_1 = \mu_2 = \mu$ in equation (3):

$$G = \frac{\mu - 1}{\mu + 2} \qquad (4)$$

Hysteresis curve data selection criteria

The most recent data reduction has resulted in the global lunar hysteresis curve shown in Fig. 3. This curve has been constructed using a total of 2703 simultaneous Apollo 12-Explorer 35 magnetometer data sets, measured during four orbits of the moon through the geomagnetic tail. (In the earlier permeability calculation (Parkin et al., 1973) a smaller quantity of 205 data sets was used, with less strict data selection criteria.)

Fig. 3

The present hysteresis curve data have been carefully selected to minimize the aforementioned contaminating induction and interaction field modes. For reasons described in the previous section, contamination from plasma diamagnetism ($\underline{B}_D$) in the extralunar environment is minimized by eliminating

data points for which the magnitude of the external magnetizing field $|\underline{H}| < 6\times10^{-5}$ Oe.

Since poloidal eddy-current induction ($\underline{B}_p$) is dependent upon time rate of change of the external field ($\partial\underline{H}/\partial t$), contamination from the poloidal mode is minimized by restricting variations in the driving field $\underline{H}$. Two-minute intervals of $\underline{H}$ and $\underline{B}$ data (with $|\underline{H}| > 6\times10^{-5}$ Oe) are examined using a computer program designed to select intervals during which the Explorer 35 and Apollo 12 data peak-to-peak variations are $< 2\times10^{-5}$ Oe and $< 1\times10^{-5}$ Oe, respectively. Data which qualify under these criteria are then averaged over the two-minute intervals, and the averages are plotted to construct hysteresis curves. For likely lunar electrical conductivity profiles (Dyal et al., 1974), the peak-to-peak criteria imposed on data, limit poloidal field induction to magnitude < 0.7 gamma. We average data over two-minute intervals, however, so that the possible error due to poloidal induction is much less than 0.7 gamma. Furthermore, since $\underline{B}_p$ is not a function of $\underline{H}$ but rather of $\partial\underline{H}/\partial t$, errors due to poloidal induction could add scatter to the linear hysteresis curve, but not change its slope. The same data-selection process has also been repeated for six-minute intervals of $\underline{H}$ and $\underline{B}$ data, with similar results. These peak-to-peak criteria have been employed both to minimize poloidal field contamination and to insure uniformity of the field $\underline{H}$ over a region larger than the distance between the Apollo 12 and Explorer 35 for all selected data.

We note here that similar peak-to-peak criteria could not be applied to simultaneous Apollo 15 LSM and Explorer 35 data since by the time Apollo 15 was deployed $1\frac{1}{2}$ years after the Apollo 12 data were taken, the Explorer 35 magnetometer data were contaminated by a spin tone modulation, of period ~ 0.8 min, which caused peak-to-peak oscillations as much as 5×10^{-5} Oe

during quiet times in the geomagnetic tail. Therefore as yet we have been unable to update the Apollo 15 results which we reported earlier (Parkin et al., 1973), and we consider only Apollo 12 data in this paper.

In our calculations of the whole moon permeability we use only results from the radial components of $\underline{B}$ and $\underline{H}$ data for several reasons. When the moon is in the geotail the Apollo 12 LSM location on the lunar surface is such that on the average, the geotail field has a radial component at least twice as large as either y or z tangential component, i.e., $H_x \gtrsim 2\, H_{y,z}$. Also, for the dipolar magnetization field $\underline{M}$, $M_x/H_x = 2\, M_{y,z}/H_{y,z}$ (see equations (1) and (2)). Therefore $M_x \gtrsim 4\, M_{y,z}$, i.e., the resolution of the magnetization field is at least four times greater using the radial component. Furthermore two contaminating field modes are minimal in the radial component. Toroidal fields $\underline{B}_T$ are not present in the x-component as explained in a previous section, and plasma interaction effects (measured in the solar wind) are much lower in the x direction at the Apollo 12 site: $B_{Fx}/B_{Fz} \sim 0.2$ and $B_{Fx}/B_{Fy} \sim 0.7$ (Dyal et al., 1972).

Global magnetic permeability and induced dipole moment

The global lunar hysteresis curve which meets data selection criteria discussed in the previous section is shown in Fig. 3. Apollo 12 averages of radial (x) components are plotted on the abscissa with simultaneous Explorer 35 averages on the ordinate; 2703 sets of selected two-minute averages are used. The gap in the center of the curve is a result of the data selection criterion which eliminates data measured when the moon is near the neutral sheet. The familiar "S" shape of the hysteresis curve degenerates at these low field values to a straight line (Ellwood, 1934) intersecting the origin. The x-component of the remanent field at the Apollo 12 site has been subtracted from the Apollo 12 data. To this data

set a least squares line has been fitted. The best estimate of the slope is 1.008 ± 0.004.

The least-squares result is obtained as follows. Since both Explorer 35 and Apollo 12 data have errors assumed to be mutually independent and Gaussian in nature, neither data set can be considered to be the independent set. For this reason two linear regression analyses have been used, one with B_x as the independent variable, and the other using H_x as the independent variable. The two regression coefficients have been calculated to be 1.005 ± 0.002 and 1.011 ± 0.002, respectively; the ± 0.002 error limits are standard errors. To get the final value we have bisected the angle between the two least-squares lines and calculated the slope of the bisector to be 1.008. The 95% confidence interval of the regression analyses is ± 0.004; therefore our calculated best estimate of the slope is 1.008 ± 0.004.

Scatter in the Apollo 12-Explorer 35 data points of Fig. 3 is primarily a result of magnetic inhomogeneities between the moon and Explorer 35, small contributions from eddy current fields, and instrumental noise and offset errors in the Apollo and Explorer magnetometers. These error sources may introduce small random fluctuations into the data which will not substantially affect the slope or intercept of the least-squares line.

From the slope we calculate global relative magnetic permeability of the moon to be $\mu = 1.012 \pm 0.006$ using equations (2) and (4). Both extrema are greater than 1.0, implying that the moon, as a whole, acts as a paramagnetic or weakly ferromagnetic sphere.

The global induced dipole moment can be calculated from the global permeability. The induced dipole moment is expressed as GR_m^3H, in units of gauss-cm^3; the hysteresis curve slope = 2G + 1. Using $R_m = 1.74 \times 10^8$ cm and geomagnetic tail field $H = 10^{-4}$ Oe, the induced dipole moment is determined

to be 2.1×10^{18} gauss-cm^3.

IRON ABUNDANCE IN THE MOON

In this section we calculate free iron and total iron abundances in the moon from the global permeability result of the preceding section. Calculations are in general dependent upon thermal and compositional models of the lunar interior, and are constrained by the known lunar density and moment of inertia.

Theory

We refer again to the two-layer model of the moon shown in Fig. 1. The core-crust boundary at $R = R_c$ is the iron Curie isotherm (assumed to be spherically symmetric); its location is a function of the thermal profile of the lunar interior. In our calculations we assume the moon is composed of a homogeneous mineral (orthopyroxene or olivine) of lunar density 3.34 gm/cm^3. Free iron grains are dispersed uniformly throughout the lunar sphere. For $R > R_c$ any free iron is ferromagnetic while at greater depths where $T > T_c$, the free iron is paramagnetic.

In the outer shell there are both ferromagnetic and paramagnetic contributions to the total magnetic permeability $\mu_1 = 1 + 4\pi k_1$. The susceptibility of the shell is $k_1 = k_{1c} + k_{1a}$, where k_{1a} is "apparent" ferromagnetic susceptibility and k_{1c} is paramagnetic susceptibility. The ferromagnetic component is metallic free iron, assumed to be composed of multidomain, noninteracting grains; the paramagnetic component is Fe^{2+} combined in the orthopyroxene or olivine rock matrix. The expected pressures and temperatures in the outer shell are such that the ferromagnetic susceptibility of iron will not be substantially altered (Bozorth, 1951; Kapitsa, 1955).

The measured ferromagnetic susceptibility of the shell material is an

apparent value which differs from the intrinsic ferromagnetic susceptibility of the iron because of self-demagnetization of the iron grains and the volume fraction of iron in the shell. The apparent ferromagnetic susceptibility k_{1a} is related to the intrinsic susceptibility k_{1f} according to

$$k_{1a} = \frac{0.01p\ k_{1f}}{1 + N\ k_{1f}} \qquad (5)$$

where N is the shape demagnetization factor of the grains and p is the volume percentage of free iron in the lunar material. For spherical iron grains $N = 4\pi/3$ theoretically, but experimentally this value is found to range from 3 to 4 (Nagata, 1961). We shall use N = 3.5 in our calculations.

Unlike the free iron, the paramagnetic iron in the rock matrix has a continuous susceptibility across the Curie isotherm. For the combined iron the susceptibility varies according to the Langevin relation:

$$k_{1c} = nm^2/3KT \qquad (6)$$

where K is the Boltzmann constant, T is absolute temperature, n is the number of ions per gram, and m is the atomic moment. m is of the order of a few Bohr magnetons μ_B; e.g., for the Fe^{2+} ion $m = 5.25\ \mu_B$ to $5.53\ \mu_B$ (Nagata, 1961).

For $R < R_c$ the lunar material is paramagnetic only, with susceptibility $k_2 = k_{2c} + k_{2a}$; k_{2c} is the contribution of paramagnetic chemically combined iron and k_{2a} is the contribution of free paramagnetic iron above the Curie temperature. Again, k_{2a} is only an apparent value and is related to k_{2f}, the paramagnetic susceptibility of free iron, by an equation similar to (5); and k_{2c} is dependent on temperature with a relationship analogous to equation (6).

Compositional and thermal models

Lunar iron abundance is determined for two compositional models of the lunar interior. Recently Kaula et al. (1974) have determined the lunar moment of inertia I to be $I/MR_m^2 = 0.3952 \pm 0.0045$, where M and R_m are lunar mass and radius, respectively. This value is approximately that of a homogeneous sphere of constant density ($I/MR_m^2 = 0.400$); therefore we assume a moon of uniform density $\rho = 3.34$ g/cm^3, i.e., we will use homogeneous compositional models.

In the first compositional model we consider the lunar sphere to be composed of orthopyroxene ($xFeSiO_3 \cdot (1-x)MgSiO_3$), where x is the mole fraction of the Fe^{2+} phase present. Free iron grains are dispersed uniformly throughout the sphere. In a second model we replace the orthopyroxene with olivine ($xFe_2SiO_4 \cdot (1-x)Mg_2SiO_4$). Pyroxenes and olivines have been reported to be major mineral components of the lunar surface fines and rock samples (Nagata et al., 1971; Zussman, 1972; Weeks, 1972), with combined iron present as the paramagnetic Fe^{2+} ion. The ferromagnetic component of lunar samples is primarily metallic iron which is sometimes alloyed with small amounts of nickel and cobalt (Nagata et al., 1972; Pierce et al., 1971). This free iron is thought to be native to the moon (because of its low nickel content) rather than meteoritic in origin (Strangway et al., 1973). Orthopyroxene and olivine models are consistent with geochemical studies (Urey et al., 1971; Wood et al., 1970; Ringwood and Essene, 1970; Green et al., 1971) and geophysical studies (Toksöz, 1974).

Since the susceptibility of free iron changes several orders of magnitude at the iron Curie temperature (T_c), a two-layer model has been used, with the core-shell boundary R_c at the Curie isotherm (see Figure 10).

The Curie isotherm location is determined from the thermal profile used for a particular model. Fig. 4 shows the dependence of T_c on depth in the moon for hydrostatic equilibrium, superimposed on temperature profiles proposed for the moon by several authors; the increased pressure of the interior will decrease the iron Curie point by about 7×10^{-3} °C per atmosphere increase in pressure (Bozorth, 1951). For the calculations that follow, we have constructed three temperature models to span the range of temperature profiles in Fig. 4. Presently we use two-layer temperature profiles for simplicity. For model profile T_1 the Curie isotherm is spherically symmetric and located at $R_c/R_m = 0.9$. Shell and core temperatures are 600 °C and 1400 °C, respectively. For the model profile T_2 the shell is 500 °C, and the core is 1300 °C, while the Curie isotherm boundary is at $R_c/R_m = 0.85$. Temperatures are 300 °C and 700 °C for shell and core of model profile T_3, which has $R_c/R_m = 0.7$.

Normally the ferromagnetism of free iron is dependent on pressure as well as temperature. At very low magnetizing field strengths such as those of the geomagnetic tail, however, the susceptibility of iron is not strongly dependent on temperature below the Curie point (Bozorth, 1951). Uniaxial stress on iron changes its susceptibility (Kern, 1961); however, hydrostatic stress should not affect the susceptibility (Kapitsa, 1955) unless, at very high pressures, there is a change in volume (Breiner, 1967). Therefore we assume that the susceptibility of uncombined lunar iron is independent of pressure. In the outer shell where $T < T_c$, we define intrinsic ferromagnetic susceptibility of the free iron to be $k_{1f} = 12$ emu/cm^3 (Bozorth, 1951), and in the core where $T > T_c$, free iron intrinsic paramagnetic susceptibility is $k_{2f} = 2 \times 10^{-4}$ emu/cm^3 (Berkowitz and ...eller, 1969; Bozorth, 1951).

Global lunar iron abundance

Using the information described in previous sections we have generated the curves shown in Fig. 5, which relate free iron abundance (q) and total iron abundance (Q) to hysteresis-curve slope, as follows. The apparent ferromagnetic susceptibility of free iron in the shell (k_{1f}) and the apparent paramagnetic susceptibility of free iron in the core (k_{2a}) are each calculated as a function of the free iron abundance (q) using equation (5). The shell-core boundary is defined by the Curie isotherm used for a particular temperature model. In addition, the mole fraction of the Fe^{2+} phase in paramagnetic rock used in the model (orthopyroxene or olivine) is constrained by q and the bulk density. Mole fraction of Fe^{2+} is related to susceptibility using the experimental data of Nagata et al. (1957) for olivine and Akimoto et al. (1958) for orthopyroxene. Furthermore, using the Langevin relation (equation (6)), we relate susceptibility of Fe^{2+} to temperature and thus find Fe^{2+} susceptibility in the shell (k_{1c}) and the core (k_{2c}) for our three temperature models. Then we combine susceptibilities to obtain total shell and core susceptibilities, $k_1 = k_{1a} + k_{1c}$ and $k_2 = k_{2a} + k_{2c}$, as a function of q, after which we use k_1 and k_2 in equation (3) to relate free iron abundance q directly to G as shown in Fig. 5. G is related to the slope of the hysteresis curve: slope = 2G + 1.

Fig. 5

We complete Fig. 5 by determining Q, the <u>total</u> iron abundance in the moon, as a function of G. Total iron Q is the combined abundance of free iron and ferrous iron. From the previously determined mole fraction of the Fe^{2+} phase in the paramagnetic mineral, we calculate the mass of ferrous iron as a function of q. Then we add the ferrous iron mass to free iron mass and get the total mass of iron in the moon, and thereby the total iron abundance Q.

We note that for $q > 1$ wt. % the susceptibility of the moon is dominated by the ferromagnetic iron (generally $k_{1a} \gg k_{1c} > k_{2c} \sim k_{2a}$) and therefore the relationship between G and q is independent of the composition of the ferrous component (olivine or orthopyroxene). Total iron abundances differ for the two compositional models because of the different iron contents of olivine and orthopyroxene.

From our measured hysteresis slope of 1.008 ± 0.004 we calculate $G = 0.004 \pm 0.002$. Using this range of G, we find from Fig. 5, free iron abundance q and total iron abundance Q for each thermal and compositional model. These iron abundances are summarized in table 1. Table 1

Fig. 5 shows the ranges of free iron and total iron abundances, which are functions of temperature in the lunar interior and are bounded by errors in the hysteresis curve slope. The lunar free iron abundance ranges between 4.5 and 0.5 wt. %; these limits correspond to thermal profiles T_1 and T_3, respectively. These thermal profiles have been selected to be upper and lower limiting cases, as can be seen upon comparison of Fig. 4 with thermal profile descriptions in the text. We accordingly calculate our free iron abundance best value as $q = 2.5 \pm 2.0$ wt. %.

Total iron abundance (Q) in the moon is, in addition, dependent upon compositional model. For the free iron/orthopyroxene model, upper and lower limits on Q are 13.7 and 11.8 wt. %, respectively; for free iron/olivine, limits are 6.8 and 4.3 wt. %. Assuming that the moon is composed of one or a combination of these minerals and has a total iron abundance between 13.7 and 4.3 wt. %, we calculate the total iron abundance best value as $Q = 9.0 \pm 4.7$ wt. %. Free iron and total iron abundances are shown in Fig. 6. Fig. 6

We note here that the susceptibilities of both olivine and orthopyroxene are about an order of magnitude too small to account for the measured lunar permeability without some ferromagnetic iron present. Also, we can calculate the minimum free iron abundance in the moon consistent with the hysteresis-curve measurements. To do this, we consider the extreme case where the measured whole-moon permeability is assumed to correspond entirely to ferromagnetic iron in the outer shell of the moon where the temperature is below the Curie point. For this case the bulk lunar iron abundance Q is 0.9 ± 0.5 wt. %. This result is independent of Curie-point depth of our three models. The extreme lower limit placed on the lunar free iron abundance by our analysis, therefore, is 0.4 wt. %.

Considerations of an iron core and iron-rich layer

The whole-moon permeability has also been used to investigate the magnetic effects of a hypothetical iron core in the moon. Density and moment of inertia measurements for the moon limit the size of such a core to less than 500 km in radius (Toksöz, 1974). If this hypothetical iron core were entirely paramagnetic and the surrounding core were orthopyroxene of average temperature 1100 °C the global permeability would be 1.0003. This value is small compared to the measured permeability of 1.012 ± 0.006, implying that if such a small paramagnetic iron core exists, its magnetization is masked by magnetic material lying nearer to the surface. Therefore the hysteresis measurements can neither confirm nor rule out the existence of a small iron core in the moon.

An iron-rich layer in the moon has been considered by several investigators (e.g., Wood et al., 1970; Urey et al., 1971; Gast and Giuli, 1972). It is possible that early melting and subsequent differention of the outer several hundred kilometers of the moon may have resulted in the formation

of a high-density, iron-rich layer beneath a low-density, iron-depleted crust. Constraints have been placed on an iron-rich layer by Gast and Giuli (1972) using geochemical and geophysical data (for example, measurements of lunar moments of inertia). One set of their models consists of high-density layers between depths of 100 km and 300 km. At a depth of 100 km the allowed layer thickness is 12 km; the thickness increases with increasing depth, to 50 km at 300 km depth. Also presented are a set of layers at 500 km depth. By using exactly the same considerations as were used in the iron abundance calculations, we calculate whole-moon permeabilities which would be expected from lunar models with these iron-rich layers. The calculations indicate that iron-rich layers allowed by geophysical constraints as outlined by Gast and Giuli, if wholly above the iron Curie temperature and therefore paramagnetic, would yield global permeabilities of about 1.00006. As for the case of a small lunar iron core, the magnetization field of such paramagnetic layers would be masked by ferromagnetic materials elsewhere in the moon, and the hysteresis curve measurements can neither confirm nor rule out these layers. This conclusion would particularly apply to the Gast-Giuli layers at 500 km depths, which would be almost certainly paramagnetic.

If the iron-rich layers existed shallow enough in the moon to be below the Curie temperature and were therefore ferromagnetic, then the measured global permeability would be about 3.5. This value is well above the upper limit for the actual measured permeability of 1.012 ± 0.006, and therefore the Gast-Giuli layers can be ruled out if they are cool enough to be ferromagnetic. It is important to note that the high-density layers discussed by Gast and Giuli (1972) can be thought of as limiting cases and that there are innumerable less dense and thinner layers which are allowed by geophysical,

geochemical and magnetic constraints.

Effects of a possible lunar ionosphere on permeability and iron abundance calculations

Measurements of the Apollo 15 subsatellite magnetometer in the geomagnetic tail have indicated the possibility that an ionosphere exists in the region between the lunar surface and the subsatellite 100 km mean altitude (Russell et al., 1974). Also, results from the Rice University suprathermal ion detector experiments indicate that charged particles measured on the lunar surface could be from a lunar ionosphere (Lindeman et al., 1973). If a global lunar ionosphere does exist, then it could form a diamagnetic region around the moon which could lower the geotail field $\underline{H}$ to a smaller magnetizing field $\underline{H}'$ and in turn result in a smaller total surface field $\underline{B}'$. Then plots of Apollo 12 data versus Explorer 35 data would be plots of B_x' vs H_x, causing the measured permeability to be lower than the true lunar permeability (in contrast to the plasma diamagnetism effect discussed earlier, which would tend to make the measured permeability higher).

If the assumption of Russell et al. (1974), that a spherically symmetric diamagnetic ionosphere fills the entire region between the lunar surface and the subsatellite 100 km altitude, were found to be correct, then our global lunar permeability would be adjusted upward. We have determined the adjusted permeability and iron abundance values by modifying equation (3) for a two-layer (shell/core) permeability model, where in this case the shell represents a lunar ionosphere of 100 km thickness and homogeneous permeability μ_i, and the core represents a lunar sphere of bulk permeability μ. The modified version of equation (3) is

$$g = \frac{(2\mu_i+\mu)(\mu_i-1) - \lambda^3(\mu_i-\mu)(2\mu_i+1)}{(2\mu_i+\mu)(\mu_i+2) - 2\lambda^3(\mu_i-\mu)(\mu_i-1)} \qquad (7)$$

where $\lambda = R_c/R_s$; R_c and R_s are radius of the core (here the lunar globe) and the outer radius of the shell (ionosphere), respectively. From the results of Russell et al. (1974) we obtain $g = -0.0101 \pm 0.0039$. Then using solutions of equations (3) and (7) we find that our permeability best value would be adjusted upward slightly from 1.012 to 1.017, provided a lunar ionosphere exists. The corresponding free iron abundance best value would be adjusted upward from 2.5 to 3.9 wt. %. Total iron content best values would be adjusted downward slightly from 12.8 to 12.1 wt. % for the free iron/orthopyroxene model, and from 5.5 to 4.7 wt. % for the free iron/olivine model. Detailed calculations of the effects of a lunar ionosphere on lunar iron content determinations will be deferred until a more detailed ionospheric model is presented.

SUMMARY AND CONCLUSIONS

(1) Simultaneous measurements by lunar magnetometers on the surface of the moon and in orbit around the moon are used to construct a whole-moon hysteresis curve, from which the global lunar relative magnetic permeability is determined to be 1.012 ± 0.006.

(2) The corresponding global induced magnetization dipole moment is expressed $\alpha = 2.1 \times 10^{22} H$. For typical geomagnetic tail fields of $H = 10^{-4}$ Oe, the corresponding induced dipole moment is 2.1×10^{18} gauss-cm^3.

(3) Both error limits on the magnetic permeability value are greater than 1.0, implying that the moon as a whole is paramagnetic and/or weakly ferromagnetic. Assuming that the ferromagnetic component is free metallic iron of multi-domain, noninteracting grains, the free iron abundance in the moon is calculated to be 2.5 ± 2.0 wt. %.

(4) A free iron abundance extreme lower limit of 0.4 wt. % is calculated under the assumption that the global susceptibility is due entirely to free iron in the ferromagnetic state. This lower limit is independent of composition of the rock matrix making up the bulk of the moon.

(5) Total iron abundance in the moon is determined by combining free iron and paramagnetic iron components for two assumed lunar compositional models, of orthopyroxene and olivine. For an orthopyroxene moon of overall density 3.34 g/cm^3 with free iron dispersed uniformly throughout the lunar interior, the total iron abundance is 12.8 ± 1.0 wt. %. For a free iron/olivine moon the total iron abundance is 5.5 ± 1.2 wt. %. A summary of iron abundance calculations is given in Table 1. Using extreme upper and lower limits in Table 1, the overall total iron abundance is expressible as 9.0 ± 4.7 wt. %.

(6) Lunar models with a small iron core and with an iron-rich layer are also discussed using the measured global lunar permeability as a constraint. A

small pure iron core of 500 km radius (the maximum size allowed by lunar density and moment of inertia measurements), which is hotter than the iron Curie point ($T>T_c$), would not be resolvable from the data since its magnetization field would be small compared to the induced field we measure. Similarly, an iron-rich layer in the moon could not be resolved if the iron is paramagnetic, i.e., the iron is above the iron Curie temperature. Gast and Giuli (1972) have proposed a family of high-density layer models for the moon which are geochemically feasible. If these models are iron-rich layers lying near the lunar surface so that $T<T_c$, the ferromagnetic layers would yield a global permeability value well above our measured upper limit. Therefore we conclude that such shallow iron-rich-layer models are not consistent with our magnetic permeability measurements.

ACKNOWLEDGMENTS

The authors are grateful to Dr. T. E. Bunch and R. T. Reynolds for many helpful discussions. Dr. T. J.Mucha, J. Arvin, K. Lewis, R. Marraccini of Computer Sciences Corporation deserve special thanks for analytical and programming support, as do Marion Legg and her group at Adia Interim Services for data reduction services. Timely assistance by D. Michniuk and L. Catalina, physics students at the University of Santa Clara, is greatly appreciated. We are pleased to acknowledge research support for C. W. P. under NASA grant no. NGR 05 017 027, and for W. D. D. under NASA grant no. NGR 45 001 040.

REFERENCES

Akimoto S., Horai K., and Boku T. (1958) Magnetic susceptibility of orthopyroxene. J. Geomag. Geoelect. 10, 7-11.

Behannon K. W. (1968) Intrinsic magnetic properties of the lunar body. J. Geophys. Res. 73, 7257-7268.

Berkowitz A. E., and Kneller E. (1969) Magnetism and Metallurgy, (Academic Press), Vol. 1.

Bozorth R. M. (1951) Ferromagnetism. D. Van Nostrand.

Breiner S. (1967) The Piezomagnetic effect on seismically active areas. Final Report No. E 22-76-67(n), Dept. of Geophysics, Stanford University.

Colburn D. S., Currie R. G., Mihalov J. D., and Sonett C. P. (1967) Diamagnetic solar-wind cavity discovered behind the moon. Science 168, 1040-1042.

Dyal P., and Parkin C. W., The Apollo 12 magnetometer experiment: Internal lunar properties from transient and steady magnetic field measurements, Proc. Second Lunar Sci. Conf., Geochim. Cosmochim. Acta, Suppl. 2, Vol. 3, 2391, MIT Press, 1971.

Dyal P., Parkin C. W., and Sonett C. P. (1970) Lunar surface magnetometer. IEEE Trans. on Geoscience Electronics GE-8 (4), 203-215.

Dyal P., Parkin C. W., and Daily W. D. Surface magnetometer experiments: Internal lunar properties, Proc. Fourth Lunar Science Conf., Geochim. Cosmochim. Acta, Suppl. 4, edited by W. A. Gose, Vol. 3, pp. 2229-2945, Pergamon, 1973.

Dyal P., Parkin C. W., and Daily W. D. (1974) Temperature and electrical conductivity of the lunar interior from magnetic transient measurements in the geomagnetic tail. Submitted to Proc. Fifth Lunar Sci. Conf., Geochim. Cosmochim. Acta, Suppl. 5, Vol. 3.

Ellwood W. B. (1934) A new ballistic galvanometer operating in high vacuum. Rev. Sci. Inst. 5, 300-305.

Gast P. W., and Giuli R. T. (1972) Density of the lunar interior, Earth Planet. Sci. Letters, 16, 299.

Green D. H., Ringwood A. E., Ware N. G., Hibberson W. O., Major A., and Kiss E. (1971) Experimental petrology and petrogenesis of Apollo 12 basalts. Proc. Second Lunar Sci. Conf., Geochim. Cosmochim. Acta, Suppl. 2, Vol. 1, pp. 601-615. MIT Press.

Hanks T. C. and Anderson D. L. (1972) Origin, evolution and present thermal state of the moon. Phys. Earth Planet. Interiors 5, 409-425.

Kapitsa S. P. (1955) Magnetic properties of igneous rock under mechanical stresses. Bull. (I.V.) Acad. Sci. USSR, Geophys. Ser. No. 6.

Kaula W. M., Schubert G., Lingenfelter R. E., Sjogren W. L., and Wollenhaupt W. R. (1974) Lunar Science V (Abstracts of the Fifth Lunar Science Conference), The Lunar Science Institute, Houston, p. 399.

Kern J. W. (1961) The effect of stress on the susceptibility and magnetization of a partially magnetized multidomain system. J. Geophys. Res. 66, 3807-3816.

Lindeman R., Freeman J. W. Jr., and Vondrak R. R. (1973) Proc. Fourth Lunar Sci. Conf., Geochim. Cosmochim. Acta, Suppl. 4 (New York: Pergamon Press), Vol. 3, p. 2889.

Mihalov J. D., Colburn D. S., and Sonett C. P. (1970) Observations of magnetopause geometry and waves at the lunar distance. Planet. Space Sci. 18, 239-258.

Nagata T. (1961) Rock Magnetism. Maruzen Co. Ltd.

Nagata T., Yukutake T., and Uyeda S. (1957) On magnetic susceptibility of Olivines. J. Geomag. Geoelect. 9, 51-56.

Nagata T., Fisher R. M., Schwerer F. C., Fuller M. D., and Dunn J. R. (1971) Magnetic properties and remanent magnetization of Apollo 12 lunar materials and Apollo 11 lunar microbreccia. Proc. Second Lunar Sci. Conf., Geochim. Cosmochim. Acta, Suppl. 2, Vol. 3, pp. 2461-2476. MIT Press.

Nagata T., Fisher R. M., Schwerer F. C., Fuller M. D., and Dunn J. R. (1972) Rock magnetism of Apollo 14 and 15 materials. Proc. Third Lunar Sci. Conf., Geochim. Cosmochim. Acta, Suppl. 3, Vol. 3, pp. 2423-2447. MIT Press.

Ness N. F., Behannon K. W., Scearce C. S., and Cantarano S. C. (1967) Early results from the magnetic field experiment on Explorer 35, J. Geophys. Res. 72, 5769-5778.

Parkin C. W., Dyal P., and Daily W. D. (1973) Iron abundance in the moon from magnetometer measurements. Proc. Fourth Lunar Sci. Conf., Geochim. Cosmochim. Acta, Suppl. 4, Vol. 3, p. 2947, edited by W. A. Gose, Pergamon Press.

Pearce G. W., Strangway D. W., and Larson E. E. (1971) Magnetism of two Apollo 12 igneous rocks. Proc. Second Lunar Sci. Conf., Geochim. Cosmochim. Acta, Suppl. 2, Vol. 3, pp 2451-2460. MIT Press.

Reynolds R. T. and Summers A. L. (1969) Calculations on the composition of the terrestrial planets. J. Geophys. Res. 74, 2494-2511.

Rich F. J., Reasoner D. L. and Burke W. J. (1973) J. Geophys. Res. 78, 8097.

Ringwood A. E. and Essene E. (1970) Petrogenesis of lunar basalts and the internal constitution and origin of the moon. Science 167, 607-610.

Russell C. T., Coleman P. J., Jr., Lichtenstein B. R., and Schubert G. (1974) Institute of Geophysics and Planetary Physics Publication No. 1269-44, Univ. of Calif. at Los Angeles.

Schubert G., and Schwartz K. (1969) A theory for the interpretation of lunar surface magnetometer data, The Moon, 1, 106.

Sill W. R., and Blank J. L. (1970) Method for estimating the electrical conductivity of the lunar interior, J. Geophys. Res. 75, 201.

Sonett C. P., Colburn D. S., Currie R. G., and Mihalov J. D. (1967) The geomagnetic tail; topology, reconnection, and interaction with the moon. In Physics of the Magnetosphere (editors R. L. Carovillano, J. F. McClay, and H. R. Radoski). D. Reidel.

Sonett C. P., Schubert G., Smith B. F., Schwartz K., and Colburn D. S. (1971) Lunar electrical conductivity from Apollo 12 magnetometer measurements: Compositional and thermal inferences. Proc. Second Lunar Sci. Conf., Geochim. Cosmochim. Acta, Suppl. 2, Vol. 3, pp. 2415-2431, MIT Press.

Strangway D. W., Gose W. A., Pearce G. W., and Carnes J. G. (1973) Magnetism and the history of the moon. Proc. of the 18th Annual Conf. on Magnetism and Magnetic Materials. J. Applied Phys. In press.

Toksoz M. N., (1974) Geophysical data and the interior of the moon, Ann. Rev. Earth and Planet. Sci, In press.

Urey H. C. (1962) The origin of the moon. In The Moon (editors Z. Kopal and Z. K. Mikhailov), pp. 133-148. Academic Press.

Urey H. C. and MacDonald G. J. F. (1971) Origin and history of the Moon. In Physics and Astronomy of the Moon (editor Z. Kopal), pp. 213-289. Academic Press.

Urey H. C. Marti K., Hankins J. W. and Liu M. K. (1971) Proc. Second Lunar Science Conf., Geochim. Cosmochim. Acta, Suppl. 2 (Cambridge, Mass.: MIT Press), Vol. 3, p. 987.

Wanke H., Baddenhausen H., Driebus G., Quijano-Rico M., Palme M., Spettel B., and Teschke F. (1973) Multielement analysis of Apollo 16 samples and about the composition of the whole moon, in Lunar Science IV, editors J. W. Chamberlain and C. Watkins, pp. 761-763, Lunar Science Institute, Houston.

Weeks R. A. (1972) Magnetic phases in lunar material and their electron magnetic resonance spectra: Apollo 14. Proc. Third Lunar Sci. Conf., Geochim. Cosmochim. Acta, Suppl. 3, Vol. 3, pp. 2503-2517, MIT Press.

Wood J. A., Dickey J. S., Marvin U. B., and Powell B. J. (1970) Proc.

Apollo 11 Lunar Sci. Conf. Geochim. Cosmochim. Acta, Suppl. 1, Vol. 1, p. 965, edited by A. A. Levinson, Pergamon Press.

Zussman J. (1972) The mineralogy, petrology and geochemistry of lunar samples -- a review. The Moon 5, 422-435.

TABLE 1 IRON ABUNDANCE OF THE MOON AS A FUNCTION OF THERMAL AND COMPOSITIONAL MODELS

	Free Iron Abundance, wt. %			Total Iron Abundance, wt. %		
thermal model / compositional model	T_3	T_2	T_1	T_3	T_2	T_1
orthopyroxene	1.0 ± 0.5	2.0 ± 1.0	3.0 ± 1.5	13.4 ± 0.3	13.0 ± 0.5	12.6 ± 0.6
olivine	1.0 ± 0.5	2.0 ± 1.0	3.0 ± 1.5	6.5 ± 0.3	5.9 ± 0.7	5.3 ± 1.0

3/1

FIGURE CAPTIONS

Fig. 1 Magnetization induction in the moon. When the moon is immersed in a uniform external field $\underline{H}$ (in this case the steady geomagnetic tail field), a dipolar magnetization field $\underline{M}$ is induced in permeable material in the lunar interior, with the dipole axis of $\underline{M}$ aligned along the direction of $\underline{H}$. The total magnetic field near the moon is $\underline{B} = \underline{H} + 4\pi \underline{M}$. The magnetic permeabilities of the two layers are μ_1 and μ_2, and for regions outside the moon, $\mu = \mu_o = 1$ (free space). $\underline{H}$ is measured by the lunar orbiting Explorer 35, whereas $\underline{B}$ is measured by an Apollo lunar surface magnetometer (LSM). Measurements of $\underline{B}$ and $\underline{H}$ allow construction of a B-H hysteresis curve for the sphere, from which permeability and iron abundance can be calculated.

Fig. 2 Magnetic environment of the moon during a lunar orbit, with emphasis on the geomagnetic tail region. The plane of the lunar orbit very nearly coincides with the ecliptic plane of the earth's orbit. The earth's permanent dipole field is swept back into a cylindrical region known as the geomagnetic tail; at the lunar distance the field magnitude is ~10 gammas (10^{-4} oersteds). Also shown is the shock surface ("bow shock") created by supersonic flow of solar wind plasma past the geomagnetic tail. Substructure of the tail consists of two "lobes"; the upper or northward lobe has its magnetic field (dark arrow) pointing roughly toward the earth, whereas the lower lobe field points away from the earth. The moon is immersed in the tail about four days of each orbit; the moon can pass through either or both lobes, depending upon the characteristics of the particular orbit and the orientation of the earth's magnetic dipole axis.

Fig. 3 Hysteresis curve for the moon. Data points are 2703 simultaneous 2-minute averages of radial components of the external geomagnetic field data $\underline{H}$ (measured by the lunar orbiting Explorer 35 Ames magnetometer) and total magnetic induction $\underline{B} = \mu\underline{H}$ ($\underline{B}$ is measured by the Apollo 12 lunar surface magnetometer). Data points are selected from four lunations of measurements made when the moon is immersed in the uniform geomagnetic tail field, far from the neutral sheet in the tail. In this low-external-field regime (~ 10 gammas or 10^{-4} Oe), the hysteresis curve is linear and is fitted by a least-squares line of slope 1.008 ± 0.004. This slope corresponds to a whole-moon magnetic permeability of 1.012 ± 0.006. The least-squares line intersects the origin exactly in this figure because the vertical-axis intercept (the radial or x-component of the remanent field at the Apollo 12 site) was subtracted out after the least-squares fit was made.

Fig. 4 Temperature profiles for the lunar interior published by various authors: (1) Hanks and Anderson (1972); (2) Dyal et al. (1974); (3) Toksöz (1974); (4) Sonett et al. (1971). Superimposed is the pressure-dependent Curie temperature for iron versus depth in the moon.

Fig. 5 Iron abundance in the moon as a function of global hysteresis curve slope. Free iron abundance (q) and total iron abundance (Q) versus the parameter G (hysteresis curve slope equals 2G+1) for three temperature profiles described in the text. Total iron abundance is shown for two lunar composition models, orthopyroxene and olivine. Arrows below the horizontal axis show the range of the parameter G, experimentally determined from the hysteresis curve slope: G = 0.004 ± 0.002. The shaded region defines the allowed values of free and total

iron abundances, bounded by hysteresis curve error limits and by thermal models T_1 and T_3.

Fig. 6 Summary of global lunar magnetic permeability and iron abundances.

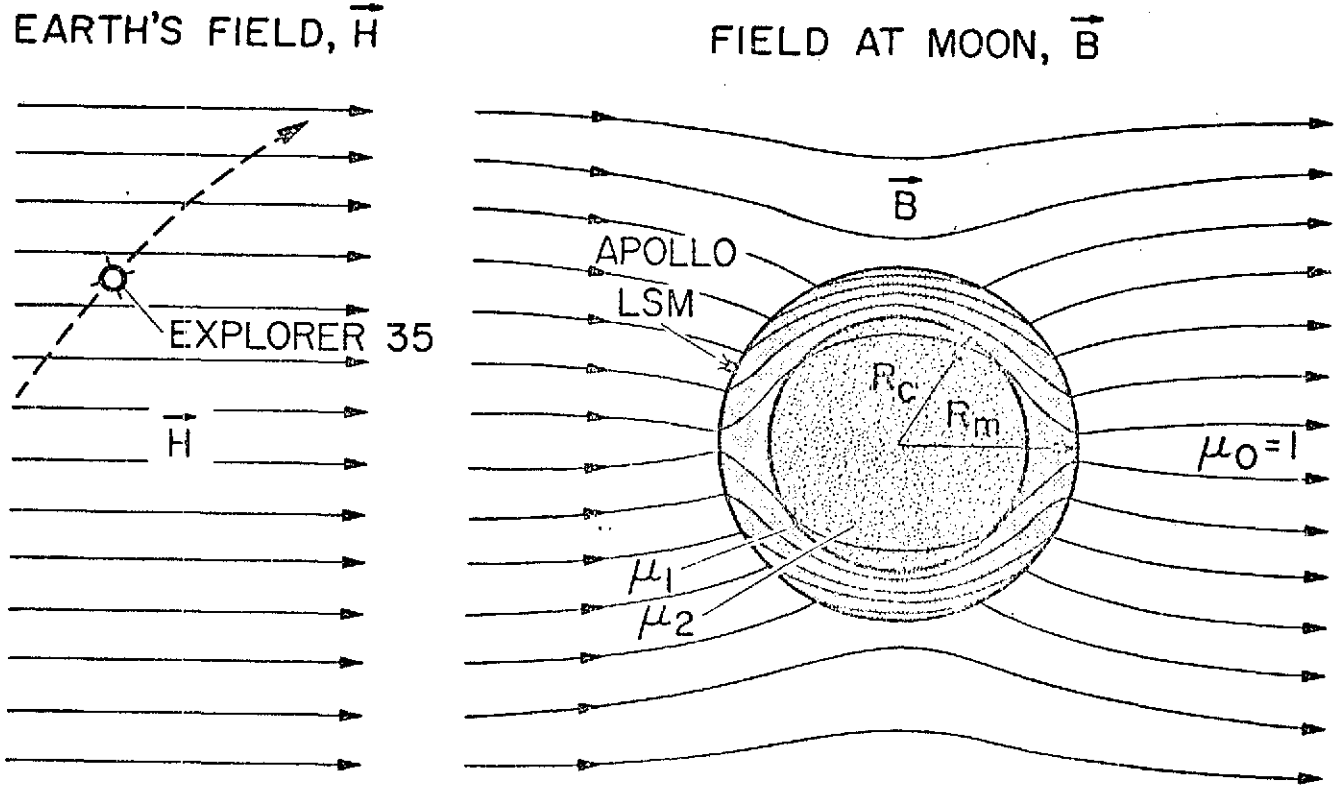
EARTH'S FIELD, $\vec{H}$
EXPLORER 35
$\vec{H}$
FIELD AT MOON, $\vec{B}$
$\vec{B}$
APOLLO
LSM
R_c
R_m
$\mu_0=1$
μ_1
μ_2

Fig. 1

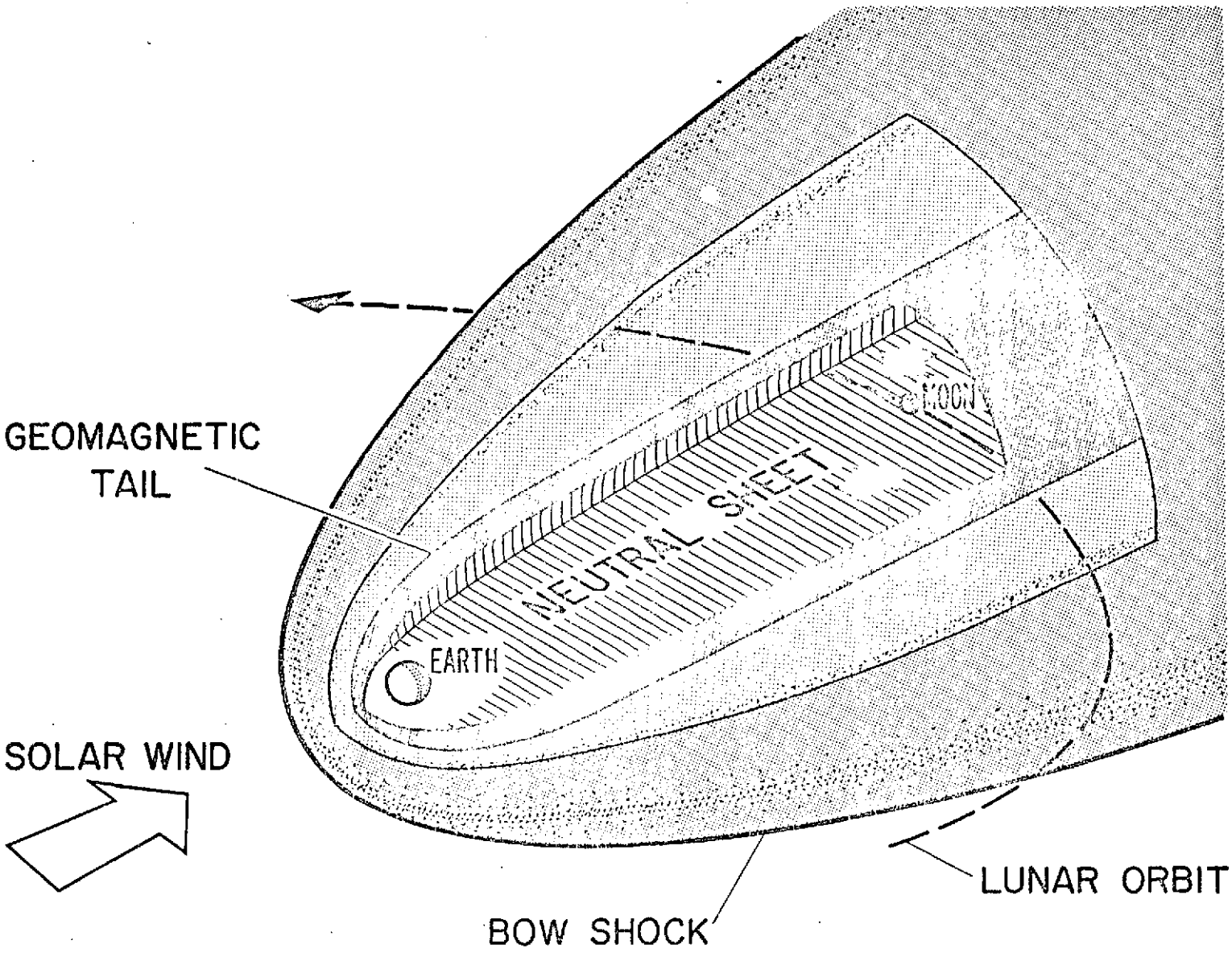
GEOMAGNETIC
TAIL
NEUTRAL SHEET
MOON
EARTH
SOLAR WIND
BOW SHOCK
LUNAR ORBIT

Fig. 2

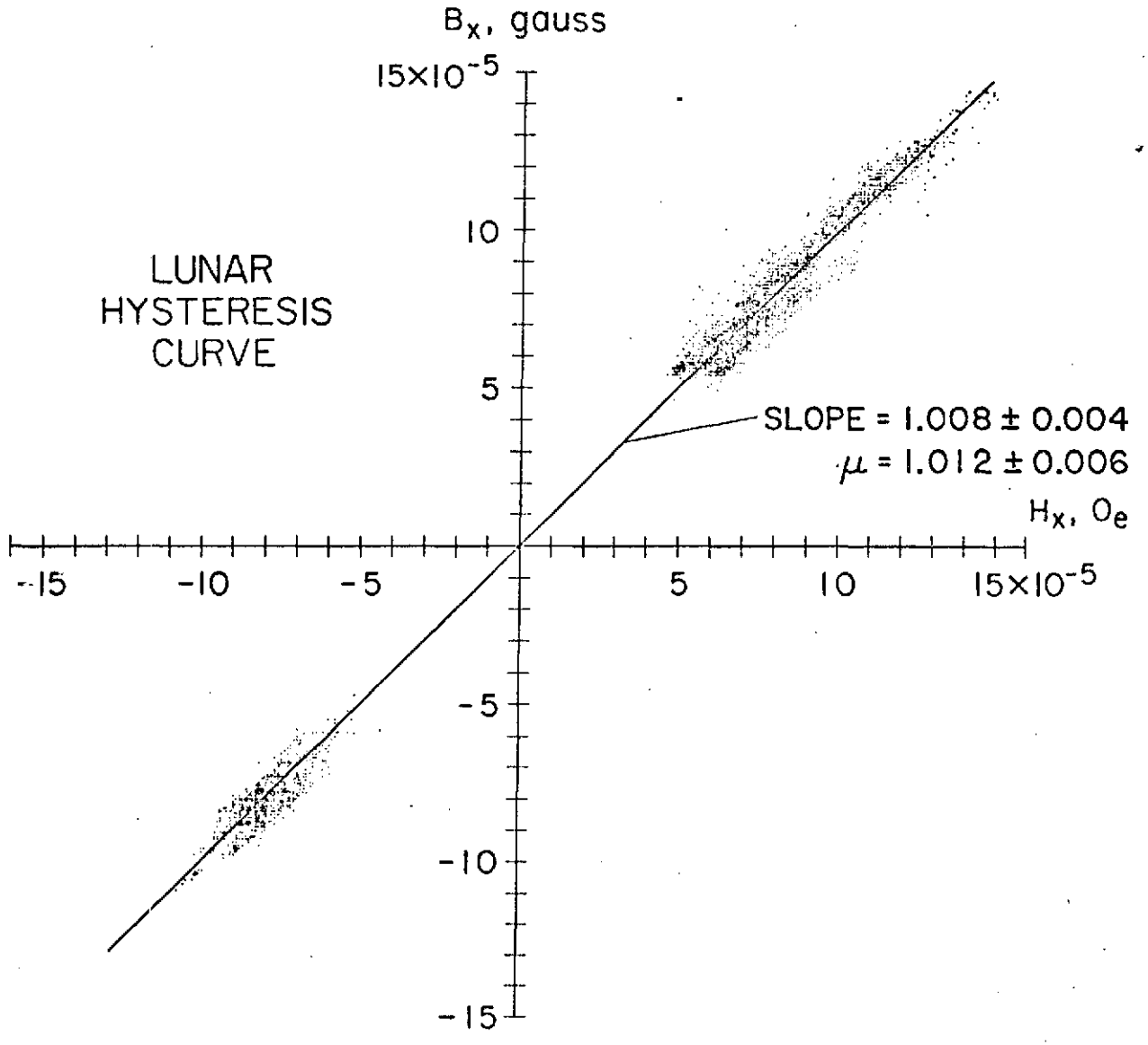
B_x, gauss
15×10^{-5}
10
5
-5
-10
-15
-15
-10
-5
5
10
15×10^{-5}
LUNAR
HYSTERESIS
CURVE
SLOPE = 1.008 ± 0.004
μ = 1.012 ± 0.006
H_x, O_e

Fig. 3

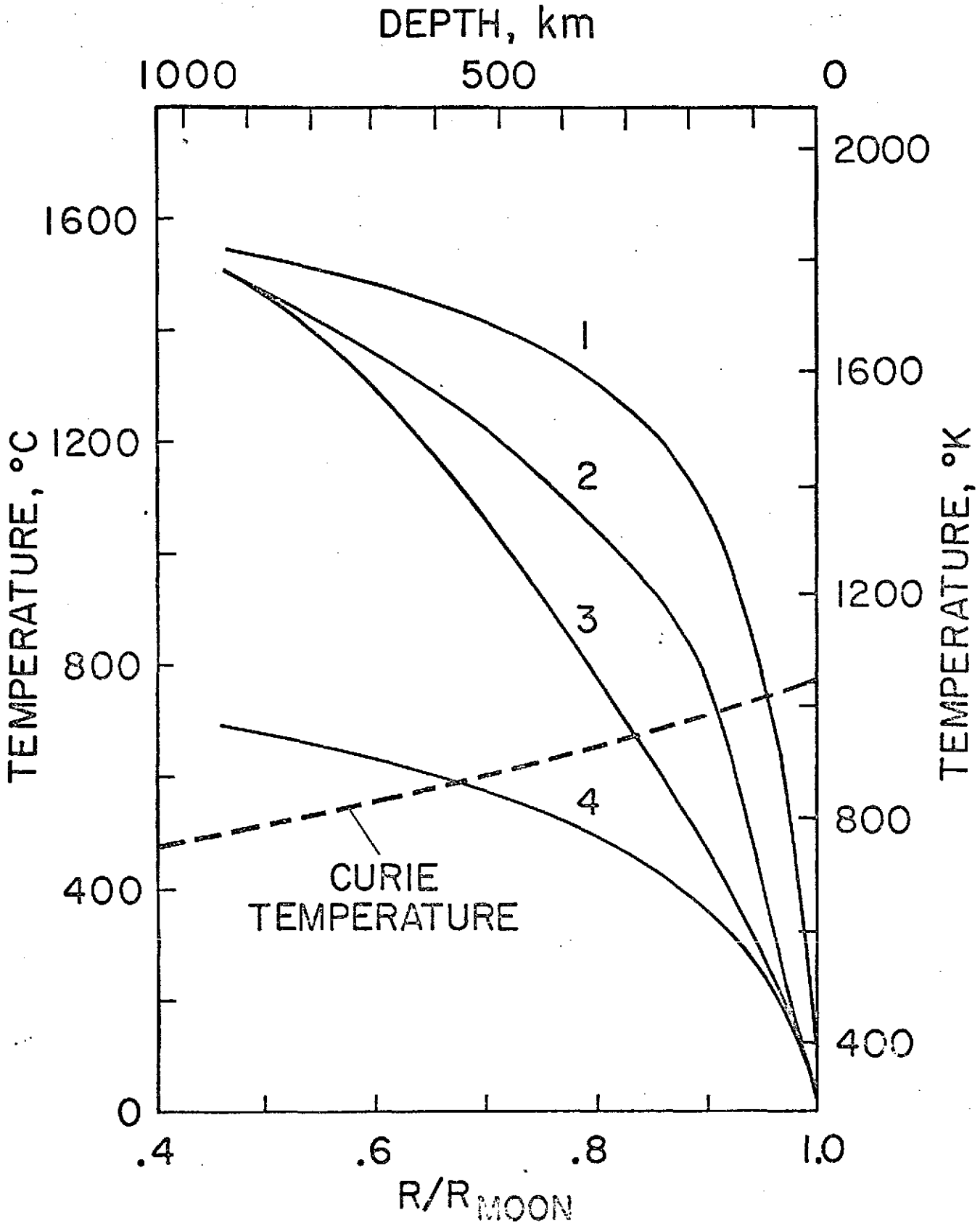
DEPTH, km
1000
500
0
2000
1600
1200
800
400
0
TEMPERATURE, °C
TEMPERATURE, °K
1
2
3
4
CURIE
TEMPERATURE
.4
.6
.8
1.0
R/R MOON

Fig. 1

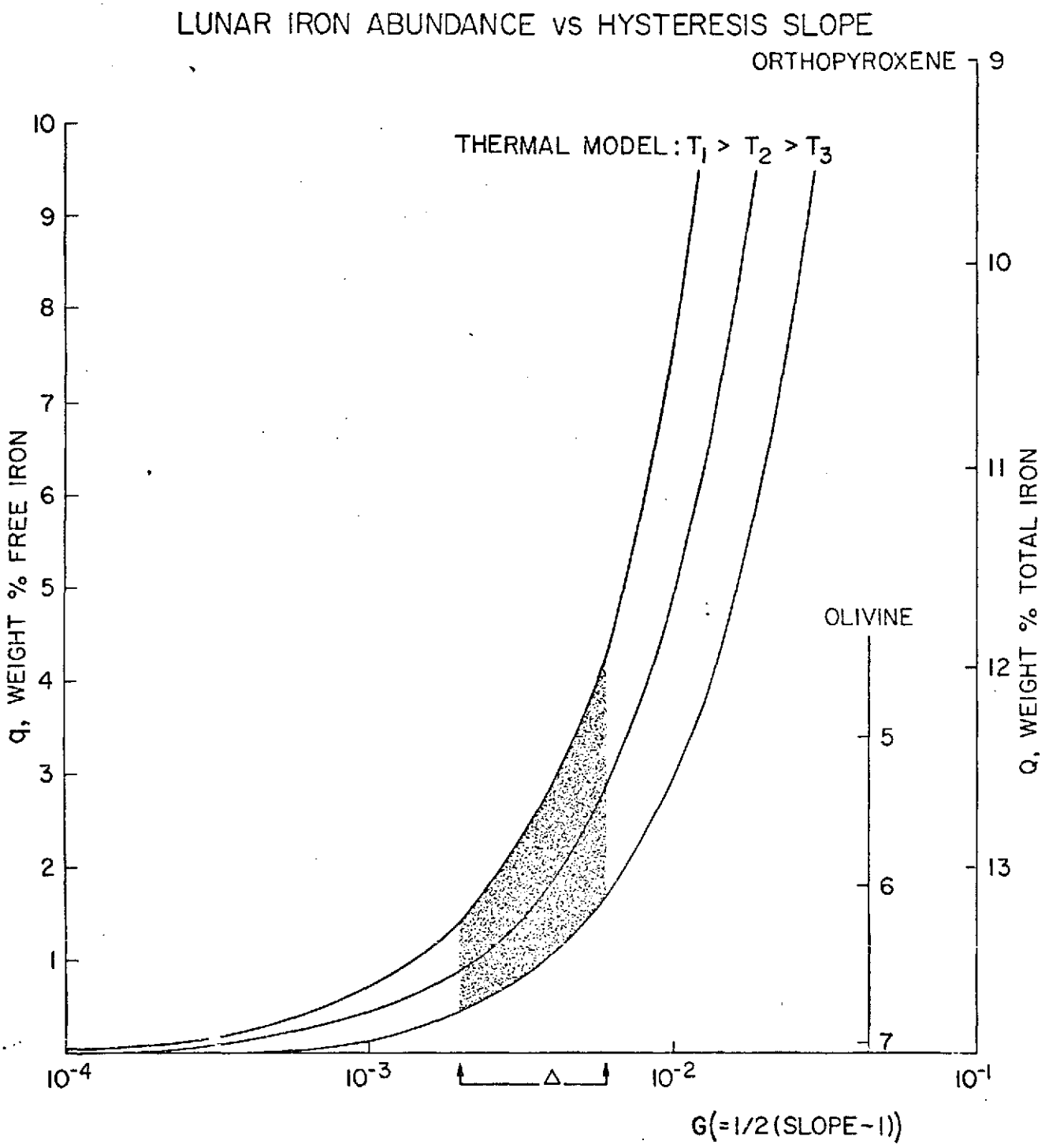
LUNAR IRON ABUNDANCE vs HYSTERESIS SLOPE
ORTHOPYROXENE
THERMAL MODEL: $T_1 > T_2 > T_3$
OLIVINE
q, WEIGHT % FREE IRON
Q, WEIGHT % TOTAL IRON
10^{-4}
10^{-3}
10^{-2}
10^{-1}
Δ
G(=1/2(SLOPE-1))

Fig. 5

LUNAR IRON ABUNDANCE

GLOBAL PERMEABILITY:	1.012 ± 0.006
FREE IRON:	2.5 ± 2.0 wt.%
TOTAL IRON:	9.0 ± 4.7 wt.%

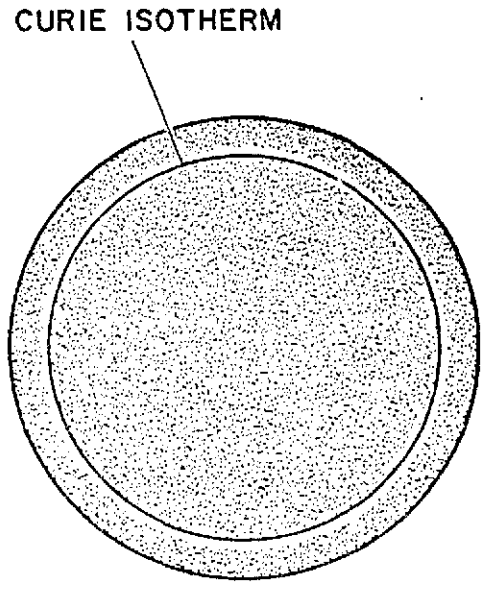

Fig. 6